Quantum Chemistry and Molecular Dynamics Simulation Study of Dimethyl Carbonate: Ethylene Carbonate Electrolytes Doped with $LiPF_6$

Oleg Borodin* and Grant D. Smith

Department of Materials Science & Engineering, 122 South Central Campus Drive, Room 304, University of Utah, Salt Lake City, Utah 84112-0560, and Wasatch Molecular Inc., 2141 St. Marys Drive, Suite 102, Salt Lake City, Utah 84108

Received: October 30, 2008

Quantum chemistry studies of ethylene carbonate (EC) and dimethyl carbonate (DMC) complexes with Li^+ and $LiPF_6$ have been conducted. We found that Li^+ complexation significantly stabilizes the highly polar cis−trans DMC conformation relative to the nearly nonpolar gas-phase low energy cis−cis conformer. As a consequence, the binding of Li^+ to EC in the gas phase is not as favorable relative to binding to DMC as previously reported. Furthermore, quantum chemistry studies reveal that, when complexation of $LiPF_6$ ion pairs is considered, the DMC/$LiPF_6$ complex is about 1 kcal/mol more stable than the EC/$LiPF_6$ complex. The EC_3DMC(cis−cis)/Li^+ complex was found to be the most energetically stable among EC_nDMC_m/Li^+ ($n + m = 4$) investigated complexes followed by EC_4/Li^+. Results of the quantum chemistry studies of these complexes were utilized in the development of a many-body polarizable force field for EC:DMC/$LiPF_6$ electrolytes. Molecular dynamics (MD) simulations of EC/$LiPF_6$, DMC/$LiPF_6$, and mixed solvent EC:DMC/$LiPF_6$ electrolytes utilizing this force field were performed at 1 M salt concentration for temperatures from 298 to 363 K. Good agreement was found between MD simulation predictions and experiments for thermodynamic and transport properties of both pure solvents and the electrolytes. We find increased ion pairing with increasing DMC content; however, both EC and DMC were found to participate in Li^+ solvation in mixed EC:DMC electrolytes despite a huge difference in their dielectric constants. In contrast to previous NMR studies, where dominance of EC in cation solvation was reported, we find a slight preference for DMC in the cation solvation shell for EC:DMC (1 wt:1 wt) electrolytes and show that reanalyzed Raman spectroscopy experiments are in good agreement with results of MD simulations. Finally, analysis of solvent residence times reveals that cation transport is dominated by motion with solvating DMC and approximately equal contributions from vehicular motions with the first solvation shell and solvent exchange with respect to solvating EC.

I. Introduction

Secondary lithium batteries with liquid electrolytes are widely used in portable electronics and are being extensively investigated for use in environmentally friendly and efficient electric vehicles and hybrid-electric vehicles.[1,2] The combination of electrode materials, electrolyte solvents, and salts strongly impacts battery performance. Electrolyte selection is a complicated task, as electrolytes should comply with a number of often conflicting requirements such as high conductivity and transference number, the ability to form a stable solid electrolyte interphase (SEI), good electrochemical and thermal stability, low flammability, volatility, and toxicity, and the ability to be produced at a low cost.

Ethylene carbonate (EC) solvent and $LiPF_6$ salt form a base for electrolyte formulations that are aimed at lithium battery applications. $LiPF_6$ salt results in electrolytes with high ion dissociation and conductivity.[2] EC-based electrolytes are known to form a stable SEI on graphitic anodes that helps prevent further electrolyte decomposition and provides good reversibility for lithium intercalation/deintercalation.[1,2] EC has a high melting point of 36.4 °C, a high dielectric constant ($\varepsilon \approx 90$), and an acceptable viscosity (1.9 cP at 40 °C).[2] Its ability to dissociate lithium salts is attributed to its high dielectric constant.[2] Addition of lower viscosity and lower dielectric constant ($\varepsilon \approx 3.1$) linear carbonate solvents such as dimethyl carbonate (DMC) decreases electrolyte viscosity, reduces its melting point, and improves conductivity. Currently, most lithium batteries utilize EC mixed with one or more linear carbonates.[2]

Due to the practical importance of EC mixed with linear carbonate solvents in lithium batteries, a large number of experimental,[2−22] quantum chemistry,[23−28] and simulation[24,29−38] studies have been published. As a result of many studies, a picture for the lithium transport and solvation in the mixed carbonate electrolytes has emerged and was outlined in the recent comprehensive review.[2] Briefly, EC dissolves lithium salts much better than DMC due to its higher dielectric constant (90 for EC vs 3 for DMC). In the EC:DMC mixture, the solvent dielectric constant gradually decreases with increasing DMC concentration. However, the question remains as to the number of EC and DMC molecules contributing to the lithium solvation shell. Intuitively, one expects EC contribution to dominate over DMC because of the difference in dielectric constants.[2] Electrospray ionization mass spectroscopy[39] and NMR spectroscopy[19] support this intuitive point of view, while Raman spectroscopy study[40] yields a different picture with a substantial contribution from both EC and DMC to the lithium solvation shell. Our goal is to provide the evidence from quantum

* To whom correspondence should be addressed. E-mail: Oleg.Borodin@utah.edu.

10.1021/jp809614h CCC: $40.75
Published on Web 01/15/2009

chemistry calculations and molecular dynamics (MD) simulations as to the picture of the lithium solvation and transport in this technologically important electrolyte.

In this study, we will perform quantum chemistry calculations in order to better understand interaction between Li^+, $LiPF_6$, EC, and DMC, and utilize these studies to develop and validate a many-body polarizable force field. This force field will be utilized in molecular dynamics (MD) simulations of EC/$LiPF_6$, DMC/$LiPF_6$, and mixed solvent EC:DMC/$LiPF_6$ electrolytes. Particular attention will be paid to the lithium cation competitive solvation by EC and DMC and how these results corroborate with the analysis of gas-phase EC_nDMC_m/Li^+ complexes utilizing quantum chemistry methods and the results obtained from analysis of the Raman spectra.[40] We will demonstrate that the intuitive picture of EC exclusively solvating Li^+ in EC:DMC(1:1) electrolyte contradicts quantum chemistry gas-phase data and results of MD simulations. Finally, electrolyte thermodynamic properties, ion transport properties, the structure of ion aggregates, and ion transport mechanisms will be extracted from MD simulations and discussed in detail.

We note that this is the first comprehensive and validated study of the mixed electrolyte composed of linear and cyclic carbonates such as EC:DMC/$LiPF_6$. Previous studies focused on single solvent electrolytes such as EC/LiTFSI,[33] DMC/LiTFSI,[35] GBL/LiTFSI,[35] oligoethers/Li salts,[41,42] acetamide/LiTFSI,[43] EC/$LiBF_4$,[31] PC/$LiBF_4$,[31] DMC/$LiBF_4$,[31] and oligoethers/$LiPF_6$.[44−46] Li et al.[24] reported studies of $LiClO_4$ in EC, PC, and EC/PC mixtures. Importantly, some of the previous simulations by Li et al. and by Soeten were only 200 and 100 ps long,[24,31] which is less than the one solvent-lithium residence time and significantly less than the lithium-anion residence time reported in this work, thus questioning if systems have been fully equilibrated. In this work, we report simulations up to 20 ns on much larger systems to ensure accuracy of reported results.

II. Quantum Chemistry Studies

The Gaussian 03 package[47] has been utilized for all ab initio calculations and density functional calculations using the M05-2X[48] functional. Calculations using the M06 density functional[48,49] were performed using Q-Chem[50] software. The M05-2X and M06 density functionals were chosen because they were shown to exhibit an improved prediction of weak, dipole, and hydrogen bonding interactions compared to traditional functionals such as BLYP and B3LYP.[48,49,51−56] Throughout this paper, we use the Dz abbreviation for the aug-cc-pvDz basis set and Tz for the aug-cc-pvTz basis set.

Quantum chemistry calculations on single EC and DMC molecules as well as EC/Li^+ and DMC/Li^+ complexes have been performed at various levels of theory and basis sets, as shown in Table 1. For all complexes, the reported binding energy is the difference in energy between the complex and the constituents of the complex (carbonate molecules and Li^+) at infinite separation. For the latter, the geometry of the isolated carbonate molecules is reoptimized; hence, the binding energies reflect a "distortion" energy associated with deformation of the carbonates from their isolated, gas-phase optimal geometries. There has been no basis set superposition correction to the reported binding energies because they have been shown to be small.[35] Two DMC conformers, namely, cis−cis denoted (cc) and cis−trans denoted (ct), illustrated in Figure 1, have been investigated. Consistent with previous results,[23,35] we find that the DMC(cc) conformer is more stable in the gas phase than the DMC(ct) conformer by about 3.16 kcal/mol at the MP2/DZ level. It is important to note that all DMC complex binding energies are reported relative to the isolated DMC molecule in the low energy cis−cis conformation.

TABLE 1: Binding Energy, Distances of EC/Li^+ and DMC/Li^+ Complexes, and Dipole Moments of EC and DMC

level of theory[a]	EC/Li^+	DMC(cc)/Li^+	DMC(ct)/Li^+
Binding Energy (kcal/mol)			
HF/Dz//MP2/Dz	−53.8	−46.3	−50.2
MP2/Dz	−47.5	−40.9	−45.2
MP3/Dz//MP2/Dz	−49.2	−42.4	−46.3
MP4 (SDQ)/Dz//MP2/Dz	−48.4	−41.8	−45.9
CCSD(T)/Dz//MP2/Dz	−48.0	−41.5	−45.6
M05-2X/6-31G*	−54.0	−47.0	−51.6
M05-2X/(EC-Dz, Li-8s4p3d)	−52.1	−44.9	−48.9
M05-2X/Dz	−51.1	−44.1	−48.0
M05-2X/Tz//M05-2X/Dz	−52.1	−45.5	−49.2
force field (FF)	−45.4	−39.3	−42.9
ΔE (MP2/Dz)-(FF)	−2.1	−1.6	−2.3
Distances (Å)			
r(Li−Oc), MP2/Dz, (FF)	1.76 (1.78)	1.76 (1.77)	1.79 (1.78)
r(Li−EO_1), MP2/Dz, (FF)	3.88 (3.91)	3.91 (3.95)	3.25 (3.25)
r(Li−EO_2), MP2/Dz, (FF)	3.88 (3.91)	3.91 (3.95)	4.03 (4.06)

Dipole Moment (D)			
	EC	DMC(cc)	DMC(ct)
M05-2X/Dz	5.68	0.34	3.76

[a] If the level of geometry optimization is not states, it is the same as the level of energy calculation. The following abbreviations are used: Dz for aug-cc-pvDz and Tz for aug-cc-pvTz.

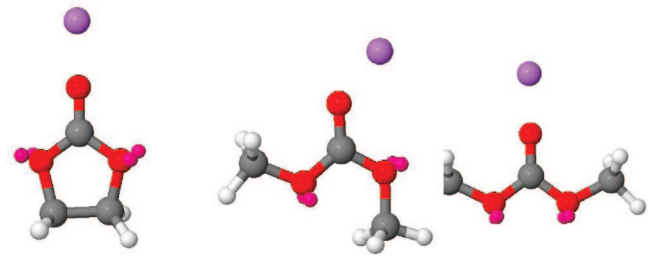

Figure 1. EC/Li^+, DMC(cc)/Li^+, and DMC(ct)/Li^+ complexes from quantum chemistry calculations. The lone pairs used in MM and MD simulations are also shown.

In accord with previously reported results,[23,35] we find that the EC/Li^+ complex is more stable than the DMC(cc)/Li^+ complex by about 6.6−7.5 kcal/mol depending on the level of theory. However, the DMC(ct)/Li^+ binding energy (relative to an isolated DMC(cc) conformer) was found to be only 2.3 kcal/mol less favorable than the EC/Li^+ binding energy at the MP2/Dz level. Despite the intrinsically higher energy of the DMC(ct) conformer compared to the DMC(cc) conformer, the larger dipole moment of DMC(ct) (3.76 D, see Table 1) results in a strong dipole−charge interaction with Li^+ yielding a more stable complex compared to the DMC(cc)/Li^+ complex. Note that the DMC(cc) conformer has a dipole moment of only 0.34 at the M05-2X/Dz level. Previous quantum chemistry studies[3,23] have focused on the less stable DMC(cc)/Li^+ complex and, thus, concluded an exaggerated stability of EC/Li^+ vs DMC/Li^+ compared to the results reported here, while Soeten[31] noticed that ∼42% of DMC molecules near lithium adopted the DMC(ct) conformation in MD simulations.

In accord with previous observations,[35] the inclusion of electron correlation (MP2 vs HF, Table 1) and increase of the

TABLE 2: Total (*E*) and Relative (to EC_3/Li^+) (ΔE) Binding Energies of Li^+ Surrounded by Three Solvent Molecules (in kcal/mol) from Quantum Chemistry Calculations at M05-2X/6-31G* Geometries and Molecular Mechanics Optimizations Utilizing the Developed Force Field

	E, M05-2X		ΔE, M05-2X			
cluster	6-31G*	Dz[a]	6-31G*	Dz[a]	*E*, FF	ΔE, FF
EC_3/Li^+	−123.8	−115.0	0.0	0.0	−103.5	0.0
EC_2/DMC(cc)/Li^+	−122.5	−111.9	1.3	3.1	−100.0	3.4
EC_2/DMC(ct)/Li^+	−120.3	−111.4	3.5	3.7	−100.8	2.6
EC/DMC$(ct)_2/Li^+$ (1st geom.)	−119.5	−109.6	4.3	5.4	−97.9	5.6
EC/DMC$(ct)_2/Li^+$ (2nd geom.)	−118.8	−109.1	5.0	6.0	−98.3	5.2
EC/DMC$(cc)_2/Li^+$	−116.6	−107.8	7.2	7.2	−96.6	6.8
DMC$(ct)_3/Li^+$	−114.7	−106.8	9.1	8.2	−96.1	7.4
DMC$(cc)_2$DMC(ct)/Li^+	−115.7	−105.7	8.2	9.3	−93.6	9.8
DMC$(ct)_2$DMC(cc)/Li^+	−114.7	−105.4	9.1	9.6	−95.3	8.1
DMC$(cc)_3/Li^+$	−110.1	−101.7	13.7	13.3	−91.1	12.4

[a] Dz = aug-cc-pvDz.

TABLE 3: Total (*E*) and Relative (to EC_4/Li^+) (ΔE) Binding Energies of Li^+ Surrounded by Four Solvent Molecules (in kcal/mol) from Quantum Chemistry Calculations at M05-2X/6-31G* Geometries and Molecular Mechanics Optimizations Utilizing the Developed Force Field

	E, M05-2X		ΔE, M05-2X			
cluster	6-31G*	Dz[a]	6-31G*	Dz[a]	*E*, FF	ΔE, FF
EC_4/Li^+	−145.3	−132.3	0	0	−119.6	0.0
EC_3DMC(cc)/Li^+	−146.6	−132.7	−1.3	−0.4	−119.5	0.1
EC_3DMC(ct)/Li^+	−143.1	−129.1	2.1	3.2	−117.0	2.6
EC_2DMC$(cc)_2/Li^+$	−145.8	−131.1	−0.5	1.2	−116.8	2.8
EC_2DMC(cc)DMC(ct)/Li^+	−142.6	−129.1	2.7	3.2	−117.1	2.5
EC_2DMC$(ct)_2/Li^+$	−140.3	−127.1	5.0	5.2	−115.7	3.9
EC,DMC$(cc)_2$DMC(ct)/Li^+	−139.9	−126.2	5.3	6.1	−113.7	5.9
EC,DMC(cc)DMC$(ct)_2/Li^+$	−139.3	−126.2	5.9	6.1	−113.5	6.1
EC,DMC$(cc)_3/Li^+$	−138.5	−125.9	6.8	6.5	−112.9	6.7
DMC$(ct)_3$DMC(cc)/Li^+	−137.8	−124.0	7.5	8.3	−111.6	8.0
DMC$(ct)_2$DMC$(cc)_2/Li^+$	−137.4	−123.7	7.8	8.6	−111.9	7.7
DMC$(cc)_4/Li^+$	−134.7	−122.1	10.6	10.2	−108.5	11.1

[a] Dz = aug-cc-pvDz.

basis set size from 6-31G* to Dz (see Table 1) decreases (makes less favorable) the EC/Li^+ and DMC/Li^+ binding energy by ~3 and ~6 kcal/mol, respectively, while further improvement of treatment of electron correlation and increase of the basis set size from Dz to Tz has only a minor influence on the binding energies. Note that in this work we performed frozen core calculations only as the inclusion of core electron correlations was shown to have only minor influence on Li^+/EC binding energies.[35] The M05-2X density functional yields results of HF and MP2, as can be seen in Table 1. The EC/Li^+ binding energy calculated using the M05-2X functional is within 0.1 kcal/mol of the previously reported[35] binding energy calculated using the B3LYP density functional using the same basis sets.

In order to understand how competitive solvation of a lithium cation by EC and DMC evolves with increasing number of carbonate molecules in the solvation shell, we performed calculations for the EC_nDMC_m/Li^+ complexes with $n + m = 3$ and 4. The M05-2X/Dz level was chosen for these calculations to reduce computation cost compared to the MP2/Dz level. On the basis of the binding energy difference between CCSD(T)/Dz//MP2/Dz and M05-2X/Dz levels shown in Table 1, we would recommend reducing (make less favorable) the EC_nDMC_m/Li^+ ($n + m = 3$ and 4) binding energies calculated at the M05-2X/Dz level by approximately 3 kcal/mol per solvent molecule coordinating a Li^+ cation.

Tables 2 and 3 summarize the EC_nDMC_m/Li^+ ($n + m = 3$, 4) binding energies calculated at the M05-2X/6-31* and M05-2X/Dz levels using the M05-2X/6-31* optimized geometries shown in Supporting Information Figures 1 and 2. Increasing the basis set size from 6-31G* to Dz decreases the EC_nDMC_m/Li^+ binding energies. This is consistent with the results for the EC/Li^+ and DMC/Li^+ complexes. The EC_3/Li^+ complex was found to be the most energetically stable among clusters of the Li^+ cation coordinated by three solvent molecules. A further increase of the cluster size from three to four solvent molecules yields an unexpected result that the EC_4/Li^+ complex is no longer the most energetically stable. The EC_3DMC(cc)/Li^+ complex becomes the most energetically stable. A more detailed analysis of Tables 2 and 3 indicates that increasing the size of the solvation shell lowers the energy for an EC substitution with DMC. Specifically, replacing the first, second, and third EC with DMC has an energy penalty of 3.1, 5.4, and 8.2 kcal/mol for EC_nDMC_m/Li^+ ($n + m = 3$) and only −0.4, 1.2, and 6.1 kcal/mol for the EC_nDMC_m/Li^+ ($n + m = 4$) complex. Interestingly, the EC_3DMC(cc)/Li^+ complex is more stable than the EC_3DMC(ct)/Li^+ complex by 3.6 kcal/mol, while the reverse trend is expected from the comparison of the DMC(cc)/Li^+ vs DMC(ct)/Li^+ binding energies. We attribute the weaker binder energy of EC_3DMC(ct)/Li^+ vs EC_3DMC(cc)/Li^+ to an unfavorable dipole−dipole interaction between EC and DMC(ct) molecules located on opposing sides of the lithium cation, while the DMC(cc) molecule, possessing a very small dipole moment, does not have such an unfavorable interaction with the EC located on the opposite side of the Li^+ (see the Supporting Information for pictures of geometries). In the case of a lithium coordinated by *three* solvent molecules, the EC_2/DMC(cc)/Li^+ and EC_2/DMC(ct)/Li^+ complexes have a similar stability at the M05-2X/aug-cc-pvDz level. Indeed, the DMC(ct) molecule

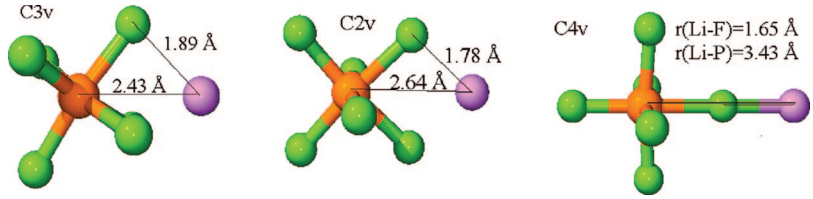

Figure 2. $LiPF_6$ optimized geometries from M05-2X/Dz quantum chemistry calculations.

TABLE 4: Li^+/PF_6^- Binding Energy and PF_6^- Distortion Energy from Quantum Chemistry and MM Calculations Using the Developed Force Field (FF) for Complexes Shown in Figure 2

	binding energy						distortion energy	
geometry optimization energy calculation	MP2/Dz[a] MP2/Dz[a]	M06/Dz[a] M06/Dz[a]	M06/cc-pvTz[a] M06/cc-pvTz[a]	M05-2X/Dz M05-2X/Dz	M05-2X/Dz M05-2X/Tz	M05-2X/Dz FF	M05-2X/Dz M05-2X/Dz	M05-2X/Dz FF
$LiPF_6$, C_{3V}	−135.8	−135.5	−138.3	−137.5	−138.2	−137.2	7.8	7.1
$LiPF_6$, C_{2V}	−132.8	−135.2	−135.6	−134.2	−135.2	−134.3	7.2	6.3
$LiPF_6$, C_{4V}	−115.0	−115.9	−118.9	−115.5	−118.1	−115.5	7.2	6.2

[a] Using [8s4p3d/5s3p2d] type basis set[57] for Li.

TABLE 5: EC/$LiPF_6$ and DMC(cc)/$LiPF_6$ Binding Energies (E) from Quantum Chemistry Calculations and MM Calculations Using the Developed Force Field

	E (kcal/mol)			$E_{EC/LiPF_6} - E_{DMC(cc)/LiPF_6}$ (kcal/mol)		
	M05-2X/6-31G*	M05-2X/Dz	FF	M05-2X/6-31G*	M05-2X/Dz	FF
EC/$LiPF_6$	−180.9	−162.7	−161.2	0	0	0
DMC(cc)/$LiPF_6$	−181.8	−163.7	−161.6	0.9	1.0	0.5

adjusts its position and orientation to minimize the unfavorable dipole−dipole interaction with EC molecules coordinating a Li^+ ion. Further examination of Table 3 indicates that, with an increase in the number of DMC molecules and a decrease in the number of EC molecules in the lithium coordination shell, we would anticipate a increasing population of DMC conformers in the cis−trans state and an decreasing population of DMC in the cis−cis state for gas-phase EC_nDMC_m/Li^+ complexes. Analysis of the Li−EC and Li−DMC complex structures indicated that the optimal Li···Oc (carbonyl oxygen) separation increases with increasing number of solvent molecules bound to a Li^+ ion in agreement with previous quantum chemistry studies.[30] At the M05-2X/6-31G* level, the Li−Oc separation increases from 1.76 to 1.92−1.93 Å for the $Li^+(EC)_n$ complexes as n increases from one to four. Interestingly, the Li−Oc(DMC) separation in the EC_nDMC_m/Li^+ ($n + m = 3, 4$) complexes is very similar to the Li−Oc(EC) separation with all Li−Oc distances being in the range 1.88−2.0 Å.

Next, we investigate the Li^+/PF_6^- binding energy and extend our previous investigation[46] of the influence of basis set on Li^+/PF_6^- binding energy to include Dz and Tz basis sets with the M05-2X and M06 density functionals for three complexes shown in Figure 2 and Table 4. The ordering of the Li^+/PF_6^- complex stability (C_{3V}, C_{2V}, and C_{4V}) is not influenced by the basis set choice and the choice of the density functional and is the same as reported previously.[46] For the most stable geometry (C_{3V}), the binding energy (relative to geometry optimized isolated PF_6^-) is in the range 136−138 kcal/mol. The M05-2X density functional tends to yield a slightly higher (more favorable) binding energy compared to the M06 density functional and MP2 (frozen core) calculations. An increase of the basis set size from Dz to Tz systematically increases the Li^+/PF_6^- binding energy by 0.7−2.6 kcal/mol. Note that all Li^+/PF_6^- binding energies for the C_{3V} geometry reported in this work are higher than the values from −132.5 to −134.3 kcal/mol obtained in our previous work[46] at the MP2 level and using the BLYP, B3LYP, and B3PW91 density functionals with a [5s2p1d] basis set[57] for Li^+ and 6-311+G(2df) basis set for PF_6^-.

Since in liquid carbonate electrolytes Li^+ is often paired with an anion,[8] it is instructive to calculate the EC and DMC binding energy not with Li^+ but with the $LiPF_6$ ion pair. These binding energies are shown in Table 5. Interestingly, the DMC(cc)/$LiPF_6$ binding energy is slightly more favorable than the EC/$LiPF_6$ binding energy, in contrast to trends observed for the EC/Li^+ and DMC(cc)/Li^+ complexes. An unfavorable dipole−dipole interaction between EC and $LiPF_6$ is likely to be responsible for the reduction of the EC/$LiPF_6$ binding energy below the binding energy for the DMC(cc)/$LiPF_6$ complex. This result suggests that in EC:DMC solutions a higher number of DMC compared to EC could be expected near Li^+ bound to PF_6^- anion compared to cations not having a PF_6^- anion in their first solvation shell. The MD simulation results presented below supported this suggestion.

III. Force Field Development

A new generation force field with improved transferability of nonbonded parameters compared to our previous force field[34,35] has been developed for EC and DMC solvents as well as Li^+/PF_6^- interaction with EC and DMC. The database of force field parameters (version f1e) is available upon request from Wasatch Molecular Inc.[58] together with the SystemGenerator tools that allow one to set up all input files needed for MD simulations. The following form of the force field relating the potential energy $U^{tot}(\mathbf{r})$ to atomic coordinates r for the ensemble of atoms has been chosen. It is split into nonbonded $U^{NB}(\mathbf{r})$ and bonded contributions as given by

$$U^{tot}(\mathbf{r}) = U^{NB}(\mathbf{r}) + \sum_{bends} U^{BEND}(\theta_{ijk}) + \sum_{dihedrals} U^{DIHEDRAL}(\phi_{ijkl}) + \sum_{improper\ dihedrals} U^{IMP}(\phi^{imp}_{ijkl}) \quad (1)$$

where the sums are over all bends, dihedrals, and improper dihedrals in the system. The contributions to the potential energy

due to bends, dihedrals, and out-of-plane bending (improper dihedrals) are

$$U^{\mathrm{BEND}}(\theta_{ijk}) = \frac{1}{2}k^{\mathrm{BEND}}_{\alpha\beta\gamma}(\theta_{ijk} - \theta^0_{ijk})^2 \quad (2)$$

$$U^{\mathrm{DIHEDRAL}}(\phi_{ijkl}) = \sum_n \frac{1}{2}k^{\mathrm{DIHEDRAL}}_{\alpha\beta\gamma\delta,n}[1 - \cos(n\phi_{ijkl})] \quad (3)$$

$$U^{\mathrm{IMP}}(\phi^{\mathrm{imp}}_{ijkl}) = \frac{1}{2}k^{\mathrm{IMP}}_{\alpha\beta\gamma\delta}(\phi^{\mathrm{imp}}_{ijkl})^2 \quad (4)$$

where θ_{ijk} and θ^0_{ijk} are the instantaneous and equilibrium bending angles for atoms i, j, and k; ϕ_{ijkl} is the dihedral angle for atoms i, j, k, and l; and $\phi^{\mathrm{imp}}_{ijkl}$ is the out-of-plane bending angle for an sp^2 center at atom j. The stiffness of these interactions is characterized by the corresponding force constants $k^{\mathrm{BEND}}_{\alpha\beta\gamma}$, $k^{\mathrm{DIHEDRAL}}_{\alpha\beta\gamma\delta,n}$, and $k^{\mathrm{IMP}}_{\alpha\beta\gamma\delta}$, respectively. The subscripts α, β, γ, and δ denote atom type for atoms i, j, k, and l, respectively.

The nonbonded energy $U^{\mathrm{NB}}(\mathbf{r})$ consists of the sum of two-body repulsion and dispersion energy terms $U^{\mathrm{RD}}(\mathbf{r})$, the energy due to interactions of fixed charges $U^{\mathrm{coul}}(\mathbf{r})$, and the polarization energy $U^{\mathrm{pol}}(\mathbf{r})$ arising from the interaction between induced dipoles with fixed charges and other induced dipoles

$$U^{\mathrm{NB}}(\mathbf{r}) = U^{\mathrm{RD}}(\mathbf{r}) + U^{\mathrm{coul}}(\mathbf{r}) + U^{\mathrm{pol}}(\mathbf{r}) = \sum_{i>j}\left(A_{\alpha\beta}\exp(-B_{\alpha\beta}r_{ij}) - C_{\alpha\beta}r_{ij}^{-6} + D\left(\frac{12}{B_{\alpha\beta}r_{ij}}\right)^{12}\right) + \sum_{i>j}\left(\frac{q_iq_j}{4\pi\varepsilon_0 r_{ij}}\right) - 0.5\sum_i \vec{\mu}_i\vec{E}^0_i \quad (5)$$

where $\vec{\mu}_i = \alpha_i\vec{E}^{\mathrm{tot}}_i$ is an induced dipole at force center i, α_i is the isotropic atomic polarizability, $\vec{E}^{\mathrm{tot}}_i$ is the total electrostatic field at the atomic site i due to permanent charges q_j and induced dipoles $\vec{\mu}_j$, ε_0 is the dielectric permittivity of a vacuum, $\vec{E}^0_i$ is the electric field due to fixed charges only, $A_{\alpha\beta}$ and $B_{\alpha\beta}$ are the repulsion parameters, and $C_{\alpha\beta}$ is the dispersion parameter for interaction between atoms i and j with atom types α and β. The term $D(12/B_{\alpha\beta}r_{ij})^{12}$, with $D = 5 \times 10^{-5}$ kcal/mol for all pair interactions, is essentially zero at typical nonbonded atomic separations but becomes the dominant term at $r_{ij} < 1$ Å, ensuring that exp-6 potential is repulsive at distances much smaller than the size of an atom. Intramolecular nonbonded interactions are included for atoms separated by three or more covalent bonds. We used Thole screening[34] ($a_T = 0.2$) that smears induced dipoles in order to prevent the so-called "polarization catastrophe" from occurring. The interaction between an induced dipole and a partial charge separated by three bonds was scaled by 0.8. Finally, for heteroatom interactions, the modified Waldman−Hagler combining rules[34] were used

$$A_{ij} = \sqrt{A_{ii}A_{jj}}\frac{B_{ij}^{\ 6}}{B_{ii}^{\ 3}B_{jj}^{\ 3}}; \quad B_{ij} = \left(\frac{2}{B_{ii}^{-6} + B_{jj}^{-6}}\right)^{1/6}; \quad C_{ij} = \sqrt{C_{ii}C_{jj}} \quad (6)$$

These combining rules have been successfully used by us for simulations of liquids,[34,59] electrolytes,[34−36] and ionic liquids and SEI components.[41,60−63]

Partial Atomic Charges. In order to establish partial atomic charges for the polarizable force field, the electrostatic potentials on a grid of evenly spaced points (~10^5 points) around the molecule in a gas phase as well as the molecular dipole $\vec{\mu}_i$ moments are obtained using ab initio quantum chemistry calculations at the MP2/Dz level of theory. Charge-bond increments are used to define partial atomic charges. The value q_i of the partial charge positioned on atom i is calculated as a sum of all charge-bond increments that involve atom i, as shown in eq 7.

$$q_i = \sum_j^{n_{\mathrm{Bonds}}} \delta_{ij} \quad (7)$$

A set of charge-bond increments ($\vec{\delta}$) was determined by minimizing the objective function

$$\chi^2(\vec{\delta}) = \sum_{i=1}^{M}\left[\sum_{j=1}^{N_{\mathrm{GRID}}}\frac{\omega^{\phi}}{N_{\mathrm{GRID}}}(\phi^{\mathrm{QC}}_{ij} - \phi^{\mathrm{FF}}_{ij}(\vec{\delta}))^2 + \omega^{\vec{\mu}}(\vec{\mu}^{\mathrm{QC}}_i - \vec{\mu}^{\mathrm{FF}}_i(\vec{\delta}))^2\right] \quad (8)$$

where ϕ^{QC}_{ij} and ϕ^{FF}_{ij} are the electrostatic potentials for the ith molecule (or complex) at the jth grid point obtained from QC calculations and the developed force field, respectively, while $\vec{\mu}^{\mathrm{QC}}_i$ and $\vec{\mu}^{\mathrm{FF}}_i$ are dipole moments for molecule i. The relative weights for fitting electrostatic potential and dipole moments ω^{ϕ}, $\omega^{\vec{\mu}}$ were set to 1.0 and 0.1, respectively. The electrostatic potential for grid points closer than the radii ($r_H = 1.8$ Å, $r_O = 1.8$ Å, $r_C = 2.5$ Å, $r_P = 2.5$ Å, $r_F = 1.8$ Å) and grid points separated from any atom further than 4 Å were excluded from the fit. Sets of molecules containing the same types of charge-bond increments were fit simultaneously. Lone pairs (Lp) have been added to oxygen atoms in the C−O−C bends, as shown in Figure 1. The length of the Lp−O bond and the Lp−O−Lp angle were fit to obtain the best description of the electrostatic potential around 1,2-dimethoxyethane (DME).

Valence Bonds. Bond lengths were set to the average of the values for the corresponding bond type obtained from QC calculations at the B3LYP/Dz level of theory for EC, DMC, DME, and so forth. The B3LYP/Dz level of theory tends to predict bond length of anions longer than experimental values, while the M06/cc-pTz level of theory yields better agreement and therefore this level of theory has been utilized to obtain bond P−F bond lengths for the PF_6^- anions. The force constant for the P−F bond was adjusted to describe the lengthening of the bond for C_{4V} symmetry complexes (see Figure 4) as previously noted.[46]

Out-of-Plane Bending and Dihedral Potentials. The out-of-plane bending and dihedral terms of the force field were determined by fitting to the relative energy profiles obtained from QC calculations at the MP2/Dz level utilizing density functional geometries for EC and DMC.

Repulsion−Dispersion Parameters. As done in our previous work,[34,35] repulsion−dispersion (R/D) parameters were determined by fitting the density and heat of vaporization of *n*-alkane (yielding parameters for carbon and hydrogen atoms),[59] fluoroalkane (yielding parameters for fluorine atoms),[59] and 1,2-dimethoxyethane (DME) (yielding oxygen atom parameters) liquids. We found that the resulting R/D parameters show excellent transferability between various compounds. For ex-

TABLE 6: Density (ρ), Heat of Vaporization (ΔH), Self-Diffusion Coefficient (D), and the Finite Size Correction to the Self-Diffusion Coefficient, D^{FSC}, Viscosity (η), and Dielectric Constant (ε)[d] for EC at 313 K and DMC at 298 K Liquids from MD Simulations and Experiments (in Parentheses)

	simulation length (ns)	ρ^{MD} (g^{exp}), $\delta\rho$%	ΔH^{MD} (ΔH^{exp}), $\delta(\Delta H)$%	$D^{MD} + D^{FSC}$ (D^{exp}), δD%	η^{MD} (η^{exp}), $\delta\eta$%	ε^{MD} (ε^{exp}), $\delta\varepsilon$%
EC	9	1302 (1321),[a] −1.5%	13.8	7.8 + 1.2 (8),[c] 13%	1.75 (1.85),[c] −5%	74.2 (89.8),[d] −18%
DMC	3	1040 (1057),[a] −1.6%	8.88 (9.01),[b] −1.4%	22 + 3.4 (26),[c] 2%	0.47 (0.59),[c] −20%	2.5 (3.09), [d] −20%

[a] Reference 74. [b] Reference 75. [c] Reference 8. The DMC experimental self-diffusion is at 303 K. [d] The dielectric constant has been calculated as described in ref 76 using eqs 4 and 10 from this reference.

TABLE 7: Composition of Simulated Electrolytes, Simulation Length, Electrolyte Density, and the Composition of the First Lithium Solvation Shell

					number of atoms within r_c of Li^+		
T (K)	N_{EC} (N_{DMC}) in the box	length of the sampling (equilibration) runs (ns)	ρ (kg m^3)	Oc (EC), r_c = 2.8 Å	Oc (DMC), r_c = 2.8 Å	$F(PF_6^-)$, r_c = 2.8 Å	$P(PF_6^-)$, r_c = 4.4 Å
			EC/LPF_6, EC:Li = 13				
298	480	7 (2)	1395	3.6		0.8	0.7
298	240	8 (6)	1397	3.6		0.8	0.7
333	480	7 (2)	1357	3.3		1.0	0.8
333	240	13(6)	1356	3.5		0.9	0.7
363	480	8 (2.4)	1328	3.3		1.0	0.8
			DMC/$LiPF_6$, DMC:Li = 10				
298	(480)	20.6 (3)	1138		2.7	1.7	1.4
298	(240)	4.3 (7)	1137		2.7	1.7	1.4
333	(480)	7.3 (3)	1091		2.5	2.0	1.6
363	(480)	6.2 (3)	1051		2.4	2.0	1.6
			EC:DMC (1:1)/$LiPF_6$, (EC + DMC):Li = 11.8				
298	128 (128)	10.6 (3)	1264	1.3	1.9	1.2	1.0
333	128 (128)	6 (2)	1224	1.4	1.8	1.3	1.0
363	128 (128)	7.6 (3)	1186	1.3	1.7	1.5	1.1
			EC:DMC (3:7)/$LiPF_6$, (EC + DMC):Li = 10.7				
298	160 (360)	6.3 (3)	1206	0.9	2.3	1.4	1.1
363	160 (360)	10.4 (4)	1124	0.8	2.1	1.5	1.2

ample, R/D parameters for the sp^2 carbon in EC and DMC were set to the same values as the parameters for generic sp^3 carbon and the carbonyl oxygen R/D parameters were set equal to the ether oxygen R/D parameters. No experimental data for EC and DMC liquids has been utilized during force field parametrization in contrast to our previous generation of the force field,[34] in which a new R/D type for the carbonyl carbon had to be introduced in order to describe thermodynamic data for carbonate liquids. Density, heat of vaporization, self-diffusion coefficients, viscosity, and dielectric constants of EC and DMC from MD simulations utilizing the developed force field are shown in Table 6. Details for the simulations are provided below. The agreement between experimental data and simulation predictions for EC and DMC liquids is similar to that reported for our previous generation force field.[34] For the lithium salt, phosphorus R/D parameters were fit to describe an ionic liquid containing PF_6^- anions that will be reported elsewhere. The Li^+/Li^+ parameters were fit to MP2/Dz quantum chemistry data for a Li^+-Li^+ complex corrected for BSSE.

The dispersion parameters (C_{ij}) for interaction of the Li^+ with PF_6^-, EC, and DMC were calculated using the combining rules given in eq 6, while the repulsion parameters for Li^+/EC were fit to three paths around the EC molecule calculated at the MP2/Dz level as in the previous work[34] and scaled to yield 1.5 kcal/mol lower (less favorable) binding energies near the minima. This adjustment was required in order to bring the degree of ion dissociation for the EC/$LiPF_6$ electrolytes to a level consistent with experimental data. The binding energy reduction by 1.5 kcal/mol is equivalent to reducing EC molecular polarizability by 8% from the gas-phase value. An ab initio analysis of medium perturbation on molecular polarizabilities suggested a general tendency of decreasing polarizabilities in solution from vacuum values by as much as 13−18% for neutral solute species.[64] Thus, the reduction of the Li^+/EC binding energy by 1.5 kcal/mol from gas-phase quantum chemistry values could be attributed to the reduction of the EC polarizability in the liquid from gas-phase values. The developed EC/Li^+ R/D parameters were utilized for DMC/Li^+ without any changes. The results of molecular mechanics (MM) calculations using the developed force field for EC/Li^+, DMC(cc)/Li^+, and DMC(ct)/Li^+ complexes are summarized in Table 1. MM calculations predict EC/Li^+, DMC(cc)/Li^+, and DMC(ct)/Li^+ binding energies 1.6−2.3 kcal/mol less favorable than MP2/Dz quantum chemistry calculations consistent with the 1.5 kcal/mol correction for the condensed-phase effects described above.

We investigated the ability of MM calculations utilizing the developed force field to predict the binding energies for Li^+ solvated by three and four carbonate molecules. The results are summarized in Tables 2 and 3. The force field yields binding energies in good agreement with quantum chemistry for these complexes. The influence of the composition (number of EC and DMC molecules) of the coordination shell on binding energy is accurately reproduced by the force field. The binding energies for the complexes from MM calculations are systematically lower than results of M05-2X/Dz calculations. This is to be anticipated as M05-2X/Dz solvent/Li^+ binding energies are consistently higher than MP2/Dz binding energies.

The Li^+/PF_6^- repulsion parameters were fit to the Li^+/PF_6^- complexes shown in Figure 2 (C_{3V}, C_{2V}, and C_{4V}) using quantum chemistry geometries. The agreement between predicted total

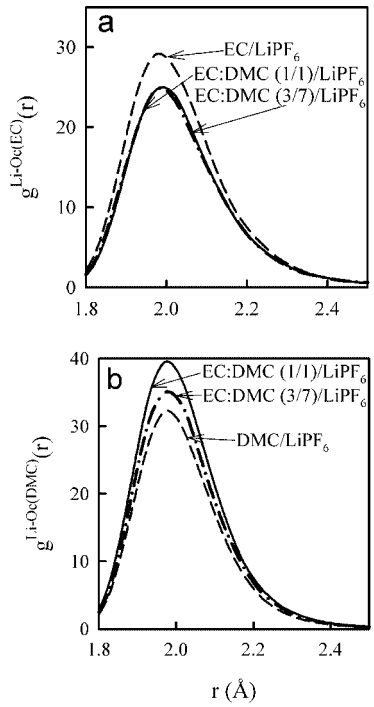

Figure 3. The Li−Oc (carbonyl) oxygen RDF for electrolytes at 298 K.

energies and the PF_6^- anion distortion energies due to its deformation upon complexation with a Li^+ cation is shown in Table 3. MM calculations have also been performed on EC/$LiPF_6$ and DMC(cc)/$LiPF_6$ complexes in order to investigate the ability of the developed force field to accurately predict EC and DMC binding energy to the ion pair as opposed to the lithium cation. As shown in Table 5, MM calculations correctly predict that the DMC(cc)/$LiPF_6$ complex is slightly more stable than the EC/$LiPF_6$ complex in agreement with the quantum chemistry results presented in Table 5.

IV. Molecular Dynamics Simulation Methodology

Four electrolyte/salt compositions were investigated, as summarized in Table 7. The solvents investigated were pure EC, pure DMC, and mixed electrolytes with equimolar mixtures of EC and DMC, denoted EC:DMC (1:1) and 30 mol % EC mixed with 70 mol % DMC, denoted EC:DMC (3:7). Each solvent was mixed with ∼1 M $LiPF_6$ at 298 K, yielding the solvent molecule to Li^+ ratios given in Table 7. Simulations were performed at 298, 333, and 363 K for all electrolytes except EC:DMC (3:7), where only 298 and 363 K were investigated. Additionally, pure DMC and pure EC solvents (without salt) were investigated at 298 and 313 K, respectively, while the salt free equimolar mixture was simulated at 298 and 333 K.

A version of the MD simulation package *Lucretius* that includes many-body polarization was used for all MD simulations.[65] A three-dimensional, periodic cubic simulation cell was used. Simulated EC/$LiPF_6$ and DMC/$LiPF_6$ electrolytes with 240 EC and 240 DMC molecules per simulation cell are denoted as small systems, while electrolytes containing 480 EC or DMC molecules per simulation cell are denoted as large systems. Simulation results for small and large systems were compared to ensure that the reported results are independent of the size of the simulation cell. All electrolytes were created in the gas phase corresponding to a cell (linear) dimension of approximately 70−95 Å. The dimensions of the simulation cells were reduced to yield estimated densities at 363 K followed by NPT (constant number of molecules, pressure, and temperature) equilibration runs, as shown in Table 7. After 2−3 ns runs at 363 K, the simulation temperature was reduced to 333 and 298 K. Sampling runs in the NVT ensemble with total trajectory lengths as given in Table 7 were then conducted. There is one important aspect that has to be taken into account during the equilibration of the DMC containing electrolytes. Because the cis ↔ trans barrier height is ∼10 kcal/mol, these transitions are uncommon on subnanosecond time scales, thus it is difficult to obtain an equilibrium distribution of cis−cis and cis−trans DMC conformers on our simulation time scale. To facilitate the equilibration process, we decreased the cis ↔ trans barrier to ∼4.5 kcal/mol in the beginning of the equilibration runs followed by a gradual increase in the barrier to the correct value over about 2 ns. Furthermore, we extended MD simulation times to 20.6 ns for DMC/$LiPF_6$ to obtain accurate statistics.

The Ewald summation method was used for electrostatic interactions between partial charges with partial charges and partial charges with induced dipole moments. The Thole screening parameter, as described in the force field section, was utilized. The interaction between an induced dipole and a partial charge separated by three bonds was scaled by 0.8, providing an improved description of the electrostatic potential around the molecules. Multiple time step integration with an inner time step of 0.5 fs (bonded interactions), a central time step of 1.5 fs for all nonbonded interactions within a truncation of 7.0 Å, and an outer time step of 3.0 fs for all nonbonded between 7.0 Å and the nonbonded truncation distance of 10.5 Å as well as for the reciprocal part of Ewald was employed. A Nose−Hoover thermostat and a barostat were used to control the temperature and pressure with the associated frequencies of 10^{-2} and 0.5×10^{-3} fs. All bond lengths except for P−F bonds were constrained using the Shake algorithm[66] in order to utilize a larger time step.

V. Electrolyte Structural Properties

We begin examination of the lithium solvation shell structure with analysis of the Li^+−Oc radial distribution functions (RDF) shown in Figure 3. Li^+ is strongly coordinated by carbonyl oxygen atoms (Oc) from EC and DMC. The position of the first peak of the Li−Oc(EC) and Li−Oc(DMC) RDF shown in Figure 3 is at ≈1.98 Å for all concentrations. This separation is consistent with optimal Li−Oc separations for the EC_nDMC_m ($n + m = 4$) gas-phase complexes, which were found to range from 1.88 to 2.0 Å in the quantum chemistry calculations discussed above. Previous simulations of EC/Li^+, EC/$LiBF_4$, and EC/$LiClO_4$,[24,31] however, reported systematically shorter Li−Oc separations, yielding first peak positions for the Li−Oc RDF at 1.7−1.96 Å. The position of the first Li−O(carbonyl) peak at 1.98 Å in this work, however, is in close agreement with the separation of 2.04 Å derived from neutron scattering experiments[22] performed on PC/$LiPF_6$ electrolytes. The magnitude of the first Li−Oc peak is around 25−40, which is about a factor of 2 smaller than the values observed in previous simulations of EC/Li^+ and EC/$LiClO_4$ performed by other groups,[24,31] thus indicating less pronounced structuring of EC in the first coordination shell of Li^+ observed in our work compared to previous simulations. Our results are in accord with the lithium first solvation shell structure for EC/LiTFSI electrolytes previously reported by us.[33] Analysis of the neutron diffraction with isotopic substitution experiments[22] for PC/$LiPF_6$ indicates that the magnitude of the first Li−Oc peak should be around ∼30, further supporting current simulation results.

Analysis of the dependence of the Li−Oc(EC) and Li−Oc(EC) RDFs on solvent composition indicates some change in the RDF

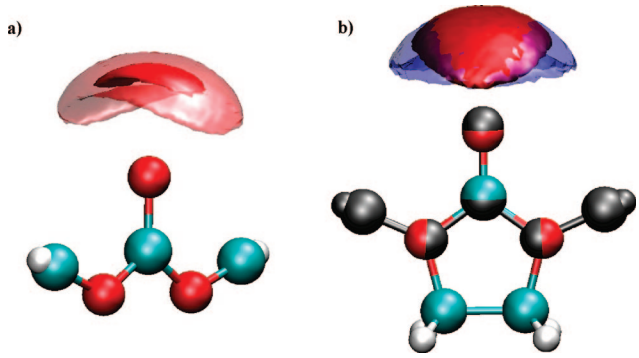

Figure 4. Li^+ cation isosurface around DMC and EC for EC/$LiPF_6$ (1 M) and DMC/$LiPF_6$ (1 M) electrolytes. Two isosurfaces are shown for DMC/$LiPF_6$ corresponding to densities of 200 (solid) and 20 (transparent) times the bulk density of lithium. The two isosurfaces shown in part b correspond to 200 times the bulk density of lithium with EC and DMC molecules superimposed on each other.

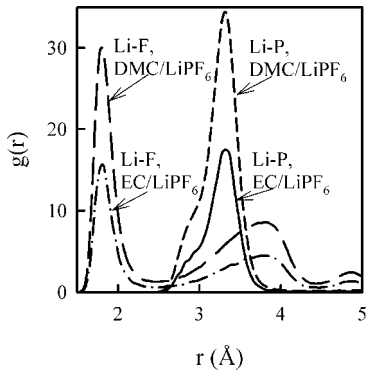

Figure 5. RDFs for EC/$LiPF_6$ (1 M) and DMC/$LiPF_6$ (1 M) electrolytes at 298 K.

first peak height by variation of the DMC:EC fraction. Both the Li−Oc(EC) RDF peak and the Li−Oc(DMC) RDF first peak decrease in height with increasing DMC content. These trends are due, at least in part, to increased participation of the anion in Li^+ solvation with increasing DMC content, as discussed below.

The spatial distribution of Li^+ near DMC and EC for the unmixed solvents + salt electrolytes was examined. The maximum value of the Li^+/DMC and Li^+/EC 3-D probability distribution functions (local density/average density) at 298 K are 380 and 280, respectively, indicating that the local lithium density at the preferred position is much higher than the average lithium density in the electrolyte. Such large values of the peak of the 3-D lithium density distribution indicate a narrow and deep energy minimum. Figure 4a shows two isosurfaces for ρ(local)/ρ(average) = 200 and 20 for lithium in DMC, indicating that reduction of the probability of finding a lithium by an order of magnitude extends the isosurface dimensions only by about a factor of 2. Figure 4b compares the isosurfaces for ρ(local)/ρ(average) = 20 for EC and DMC, demonstrating that Li^+ tends to have a much broader distribution in the plane of the molecule for EC than for DMC. A wider distribution of lithium near the carbonyl oxygen shown in the 3-D density distributions for EC corroborates well with a shift in the most probable Li···Oc−Cc angle from 157° for DMC/$LiPF_6$ to 150° for EC/$LiPF_6$.

The Li^+/PF_6^- RDFs for the unmixed electrolytes are shown in Figure 5. The first Li−F peak is located at 1.83 Å, which is a similar distance to the first Li−O(carbonyl) peak at 1.98 Å, for both the EC/$LiPF_6$ and DMC/$LiPF_6$ electrolytes as well as the mixed electrolytes (not shown). The second Li−F peak is located at ~3.8 Å. The Li−F peak magnitude is significantly larger for the DMC/$LiPF_6$ compared to EC/$LiPF_6$, indicating much greater propensity for the Li^+/PF_6^- to form contact ion pairs and aggregates in DMC solvent compared to EC solvent. A similar trend is observed for the Li−P RDFs shown in Figure 5. We find that addition of EC systematically decreases the magnitude of the Li−F and Li−P RDF peaks, indicative of salt dissociation with addition of EC.

Understanding competitive solvation of a lithium cation by EC and DMC in mixed EC:DMC electrolytes has received some attention in the literature. Interpretation of the Raman spectrum changes[40] for the C−O stretching band of EC and DMC in EC:DMC/$LiCF_3SO_3$ and EC:DMC/$LiPF_6$ electrolytes with increasing salt concentration suggested that both EC and DMC participate in solvation of Li^+ with greater participation by EC. Specifically, experiments were performed at EC:DMC (1:1 vol/vol) corresponding to 1.3:1 mol/mol. Analysis of the 720 cm^{-1} band for EC solvated by Li^+ and the 920 cm^{-1} DMC/Li^+ band indicated a similar fraction of EC and DMC in the lithium solvation shell, while more EC would be expected if random solvation by EC and DMC is assumed at the mole ratio of EC:DMC = 1.3. However, the authors cited computational evidence for greater affinity of Li^+ to EC compared to DMC based upon EC/Li^+ and DMC(cc)/Li^+ binding energies and preferred to analyze the Raman shift for EC at ~900 cm^{-1}. That analysis yielded 1.1−1.3 DMC and 2.6−3.2 EC molecules for EC:DMC = 1.3 (mol/mol) composition, indicating a greater number of EC molecules in the lithium first coordination shell. Results from Raman experiments disagree with analysis of ^{13}C NMR studies[9,19] of PC:DMC/$LiPF_6$ electrolytes that found the chemical shift of PC changing to a much greater extent than that of DMC with variation of the PC/DMC ratio, indicating no DMC affected by lithium cations. Interestingly, the chemical shift of another linear carbonate (EMC) in EMC/MP (methyl propionate) was very small despite EMC being concluded to participate in the lithium solvation,[6] thus leaving a possibility that the chemical shift of DMC is not very sensitive to the lithium coordination.

Because our developed force field predicts the binding energies of EC_nDMC_m/Li^+, EC/$LiPF_6$, and DMC/$LiPF_6$ complexes in excellent agreement with quantum chemistry studies, we feel that MD simulations utilizing this force field are sufficiently reliable to provide important insight into competitive lithium solvation by DMC and EC. The composition of the first lithium coordination shell from simulations is summarized in Table 7 for small and large simulation boxes. A solvent molecule or anion is determined to participate in the first coordination shell of a lithium whenever the Li^+−X (X = Oc, F, or P) is smaller than the corresponding cutoff distance given in Table 7. We find good agreement for the composition of the lithium solvation shell between large and small simulation boxes. The total number of molecules (solvent + anion based on fluorine) in the lithium first solvation shell is nearly independent of solvent composition and temperature, ranging from 4.3 to 4.6 for the systems studied. The total number of solvent molecules (EC + DMC) involved in the Li^+ first solvation shell decreases with increasing DMC content while the number of anions increases, indicating greater ion pair and aggregate formation with increasing DMC content. For the mixed electrolytes, we find that both EC and DMC participate in Li^+ solvation, with a noticeable but not strong preference (compared to the solvation shell composition expected for random solvation) for DMC−Li^+ coordination.

Our predictions clearly qualitatively support conclusions drawn from Raman spectroscopy experiments that DMC

TABLE 8: Raman Frequencies and Activities Calculated at the M05-2X/aug-cc-pvDz Level

	EC	EC/Li^+	DMCcc	DMCcc/Li^+	DMCct	DMCct/Li^+
Raman activity	14.1	18.5	12.8	10.9	13.1	10.95
Raman shift	924	952	957	998	899	923
Raman shift scaled by 0.97	896	923	928	968	872	895

participates in Li^+ solvation in mixed EC:DMC electrolytes, and not conclusions from ^{13}C NMR experiments that Li^+ does not interact appreciably with DMC. However, the question remains as to why Raman spectroscopy appears to indicate a higher probability (than given by random solvation) of finding an EC vs DMC participating in the solvation of Li^+ and our simulations indicate the opposite behavior. We note that experimental analysis relied on the assumption that the Raman activity of the Li^+-shifted bands is the same as that of the nonshifted band in the pure solvent. We have calculated Raman frequencies and intensities in the range of $\sim$900 cm^{-1}, as shown in Table 8, to compare with Raman experiments. The gas-phase calculated frequencies were scaled by a commonly used factor[40] of 0.97. The resulting frequencies of 928 cm^{-1} for DMC(cc) and 896 cm^{-1} for EC were found to be in good agreement with the experimentally observed values of 925 and 900 cm^{-1}. Solvent binding to Li^+ results in a blue shift in agreement with experimental data. Analysis of changes in Raman activity indicates that it increases for EC/Li^+ vs EC by 31% but decreases for DMC/Li^+ vs DMC by 12%. Utilizing our coordination numbers of DMC = 1.9 and EC = 1.32 for the EC:DMC (1:1) electrolyte at 298 K, the closest system to the experimentally measured EC:DMC (1:1.3) electrolyte that we have simulated, we would obtain coordination numbers of DMC = 1.56 and EC = 1.66 for EC:DMC (1:1)/$LiPF_6$ 1 M if we normalized the actual intensities by activities associated with nonshifted bands. As was concluded from analysis of the Raman experiments, we would conclude (incorrectly) that there is a preference for EC over DMC in the Li^+ solvation shell. Another factor that was missed during analysis of the Raman spectra is the presence of DMC(ct) conformer that exhibits a Raman shift at lower wave numbers compared to DMC(cc). Indeed, addition of 1 M $LiPF_6$ salt increases the DMC(ct) population from 4.6 to 9.4%, or approximately by 5%. A significant fraction of these DMC(ct) molecules is solvated by lithium cations and contributes to the band at 895 cm^{-1} (scaled by 0.97, see Table 8), which coincides with the frequency of EC not bound to Li^+. Thus, during Raman spectra analysis, this fraction of DMC(ct) molecules was completely omitted, resulting in a lower number of DMC molecules in the lithium solvation shell.

Next, we analyzed the influence of PF_6^- anion in the first coordination shell on the lithium solvation shell composition. In particular, we are concerned with the number of EC and DMC molecules involved in solvating Li^+ forming a "free" Li^+, a Li^+/PF_6^- contact ion pair, and a Li^+ participating in a larger ion aggregate. The probability of finding various compositions of the first lithium solvation shell for the EC:DMC (1:1) mixed electrolyte is shown in Table 9. For lithium solvation shells that do not include any PF_6^- anions, we observe approximately equal probabilities of finding EC and DMC, in particular, the probability (p) for $p(EC_nDMC_m) \approx p(DMC_nEC_m)$, $n + m = 4$. For the somewhat less likely case of $n + m = 5$, we observe a preference for EC over DMC to participate in lithium solvation. When one or more PF_6^- anions coordinate Li^+, the composition of the lithium solvation shell changes and we observe a clear trend favoring DMC molecules over EC molecules in the lithium first solvation shell. This trend can be rationalized in light of the quantum chemistry results for EC/Li^+ and DMC/Li^+ vs EC/$LiPF_6$ and DMC/$LiPF_6$ complexes shown in Tables 1 and 5, respectively, that demonstrated that the presence of PF_6^- bound to Li^+ stabilizes the binding energy of DMC vs EC. In order to further explore this supposition, we performed an 8 ns simulation of the EC:DMC(1:1)/$LiPF_6$ (1 M) electrolyte at 298 K with increased Li^+/PF_6^- repulsion interactions that resulted in a complete dissociation of Li^+/PF_6^- ion pairs. In this completely dissociated electrolyte, we found an equal amount of EC and DMC in the first lithium solvation shell.

TABLE 9: Probability (in %) of Finding Various Compositions of the First Lithium Solvation Shell[a,b]

	probability (%)				
	$n_{EC} = 0$	$n_{EC} = 1$	$n_{EC} = 2$	$n_{EC} = 3$	$n_{EC} = 4$
			$n(PF_6^-) = 0$		
$n_{DMC} = 0$					0.6
$n_{DMC} = 1$				3.7	1.8
$n_{DMC} = 2$			6.4	4.8	
$n_{DMC} = 3$		3.8	3.9		
$n_{DMC} = 4$	0.2	0.6			
			$n(PF_6^-) = 1$		
$n_{DMC} = 0$				1.9	
$n_{DMC} = 1$		0.5	10.2	1.1	
$n_{DMC} = 2$	0.2	20.4	3.1		
$n_{DMC} = 3$	8.7	2.6			
$n_{DMC} = 4$	0.4				
			$n(PF_6^-) = 2$		
$n_{DMC} = 0$			0.8		
$n_{DMC} = 1$	0.4	7.2	0.3		
$n_{DMC} = 2$	12.2	0.6			
$n_{DMC} = 3$	0.2				

[a] A solvent (EC and DMC) molecule is considered a part of the lithium first solvation shell if the distance between Li^+ and carbonyl oxygen is less than 2.8 Å. A PF_6^- anion is a considered to be a part of the lithium coordination shell if $r(Li-P) < 4.4$ Å. [b] Only probabilities greater or equal to 0.2% are shown.

We now turn our attention to the analysis of cation/anion coordination and formation of ion aggregates. Despite the high dielectric constant of EC (see Table 6), the EC/$LiPF_6$ 1 M electrolyte at 298 K still has 0.7 PF_6^- anions on average in the first solvation shell of each Li^+, as shown in Table 7. This number increases dramatically for the low dielectric constant DMC, where it can be seen that the DMC/$LiPF_6$ 1 M electrolyte at 298 K has 1.4 PF_6^- anions in the lithium first solvation shell. These trends are in qualitative agreement with analysis of Raman and IR spectroscopic measurements[67] on DMC/$LiPF_6$ and PC/$LiPF_6$ electrolytes. The mixed EC:DMC electrolytes exhibit an approximately linear increase in the number of anions coordinated with each cation with increasing DMC content. Further analysis of Table 7 indicates that the ratio of F/P atoms involved in Li^+ coordination ranges from 1.2 to 1.3. From Figure 2 and Table 4, we recall that the most energetically stable $LiPF_6$ geometry in the gas phase has C_{3V} symmetry with three fluorine atoms coordinating the Li^+. Because F/P = 1.2−1.3 in our electrolyte simulations, we conclude that the C_{3V} type of $LiPF_6$ coordination rarely happens in the condensed phase. In fact, the most dominant type of $LiPF_6$ coordination is of C_{4V} (see Figure 2) symmetry in the liquid electrolyte with some contribution from C_{2V} type coordination. Figure 6 shows an isosurface

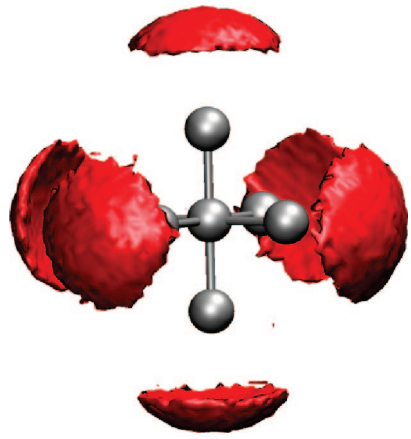

Figure 6. Li^+ cation isosurface around PF_6^- anions.

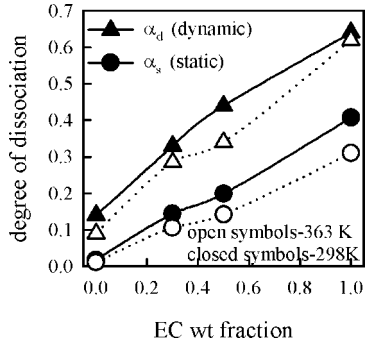

Figure 7. Dynamic (α_d) and static (α_s) degrees of ion dissociation (fraction of free ions).

of Li^+ density around PF_6^- from MD simulations of DMC/$LiPF_6$ at 298 K, supporting this conclusion. Additional support for this conclusion comes from comparison of the Li^+-P RDF in Figure 5 with the optimized $LiPF_6$ geometries in Figure 2. The preferred Li^+-P separation observed in Figure 5 is quite similar to that seen for the C_{4V} $LiPF_6$ complex. Interestingly, it was observed[46] that the metastable LiF formation occurs while Li^+ is approaching PF_6^- along the C_{4V} symmetry axis and not the C_{3V} and C_{2V} types of geometries (see also Figure 2).

The degree of ion dissociation (static) defined as the fraction of Li^+ and PF_6^- with no counterion in their first solvation shell, i.e., $r(Li-P) > 4.4$ Å for all pairs, is shown in Figure 7. From Figure 7, it can be seen that the fraction of free ions increases nearly linearly with increasing EC fraction in electrolyte and that increasing temperature slightly decreases the fraction of free ions. Surprisingly, the DMC/$LiPF_6$ 1 M electrolyte, which exhibits reasonable DC conductivity (see below), has a very low fraction of free ions (1.7% at 298 K). We also calculated the fractions of free cations and anions separately and found the fraction of free lithium higher than compared to the fraction of free anions. For example, for EC/$LiPF_6$ at 298 K, we obtained 44% for the fraction of free lithium and 38% for free PF_6^-, while, for DMC/LiPF6 at 298 K, we found 2.4% for free Li^+ and 0.7% for free PF_6^-.

Due to the low fraction of free ions, it is likely that charged ion clusters significantly contribute to charge transport for DMC containing electrolytes. The probability of an ion to participate in a cluster of n ions is shown in Figure 8 for all electrolyte compositions investigated at 298 K. $P(n = 1)$ shows the fraction of dissociated ions, $P(n = 2)$ for ion pairs, and so forth. Unexpectedly, the fraction of ions participating in contact ion pair formation stays approximately the same (~40%) for all electrolyte compositions from EC/$LiPF_6$ to DMC/$LiPF_6$, while

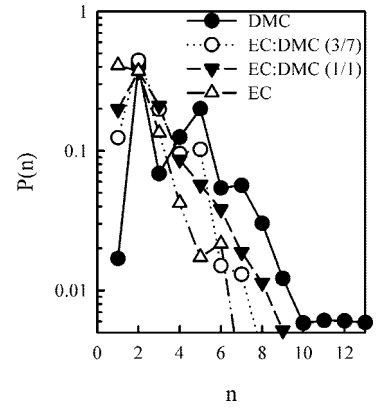

Figure 8. Probability of an ion to belong to the cluster size n for electrolytes at 298 K.

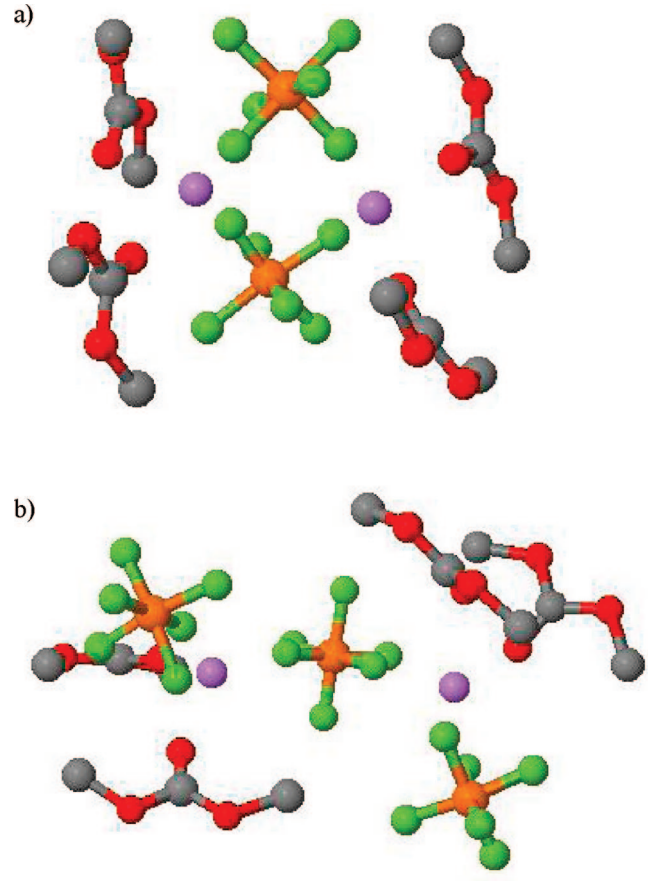

Figure 9. Representative snapshots of PF_6^- anions bridged by lithium cations.

the fraction of ions participating in larger aggregates systematically increases with increasing DMC fraction of the EC:DMC solvent. Only clusters of three ions do not follow this trend. In accord with our previous analysis of an EC/LiTFSI electrolyte,[33] we find that ion clusters of three and five have a diffusion coefficient within a factor of a few of the "free" (uncomplexed by counterions) Li^+; therefore, we expect these large ion clusters to significantly contribute to charge transport for high DMC content electrolytes where the fraction of ions participating in large clusters is significant. Visual examination of the atomistic details of the ion aggregate structure revealed that PF_6^- anions are bridged either by two lithium cations, as shown in Figure 9a, or via one lithium cation, as shown in Figure 8b, forming more extended ion aggregates. Statistical analysis indicated that both structures have approximately equal occurrences.

VI. Transport Properties

Transport properties of simulated electrolytes are calculated and discussed in the following order: ion self-diffusion coefficients, electrolyte viscosity, dynamic degree of ion correlation, and conductivity. The self-diffusion coefficient D_i for species i was calculated using the Einstein relation

$$D_i = \lim_{t\to\infty} \frac{\langle \mathrm{MSD}(t)\rangle}{6t} \tag{9}$$

where MSD(t) is the mean-square displacement of a molecule (of type i) center of mass during time t and $\langle\rangle$ denotes an ensemble average. Due to the finite size of the simulation cell, long-range hydrodynamic interactions restrict diffusion.[68] The leading order finite size correction (FSC) to self-diffusion coefficient (change to delta ΔD^{FSC}) was found to be inversely proportional to the simulation box and is given by[68]

$$\Delta D^{\mathrm{FSC}} = \frac{2.837 k_{\mathrm{B}} T}{6\pi\eta L} \tag{10}$$

where k_{B} is the Boltzmann constant, T is the temperature, L is a linear dimension of the simulation periodic cell, and η is the viscosity. The finite size correction is around 10−16% for the simulated electrolytes. For salt containing simulated systems, the correction was calculated using eq 10 and first applied to the solvent. Ion self-diffusion coefficients of Li^+ and PF_6^- were corrected by the same relative value as the solvent, typically between 1.11 and 1.17, resulting in an increase of ion transport by 11 and 17%, respectively.

The viscosity was calculated using the Einstein relation including both diagonal and nondiagonal elements to enhance statistics[69−71]

$$\eta = \lim_{t\to\infty} \frac{V}{20 k_{\mathrm{B}} T t} \langle \sum_{\alpha,\beta} (L_{\alpha\beta}(t) - L_{\alpha\beta}(0))^2 \rangle \tag{11}$$

where $L_{\alpha\beta}(t) = \int_0^t P_{\alpha\beta}(t')\,\mathrm{d}t'$, k_{B} is the Boltzmann constant, T is temperature, t is time, V is the volume of the simulation box, and $P_{\alpha\beta}$ is the symmeterized and traceless stress sensor given by eq 12

$$P_{\alpha\beta} = \omega_{\alpha\beta}\left(\frac{\sigma_{\alpha\beta} + \sigma_{\beta\alpha}}{2} - \frac{\delta_{\alpha\beta}}{3} tr(\sigma)\right) \tag{12}$$

where $\sigma_{\alpha\beta}$ is the stress tensor, $\omega_{\alpha\beta} = 1$ for $\alpha \neq \beta$, $\omega_{\alpha\beta} = {}^4/_3$ for $\alpha = \beta$, $\delta_{\alpha\beta} = 1$ for $\alpha = \beta$, and $\delta_{\alpha\beta} = 0$ for $\alpha \neq \beta$.

The self-diffusion coefficients and viscosity of the pure solvents are given in Table 6 and are in excellent agreement with pgse-NMR experiments[8] and reference viscosity data. For pure solvents at 298 K, the DMC self-diffusion coefficient is a factor of 3 higher than the EC self-diffusion coefficient at 313 K. In the mixed solvent (EC:DMC = 1wt/1wt) at 298 K, however, the self-diffusion coefficients of EC and DMC are approximately the same, specifically 15×10^{-10} and 18×10^{-10} (m^2/s), respectively, and lie between the values for pure EC and pure DMC. Similar trends were observed for DME/PC electrolytes from experiment.[72] Addition of 1 M $LiPF_6$ decreases EC and DMC self-diffusion coefficients for the pure solvent and mixed solvent electrolytes by approximately a factor of 2 as expected.[73]

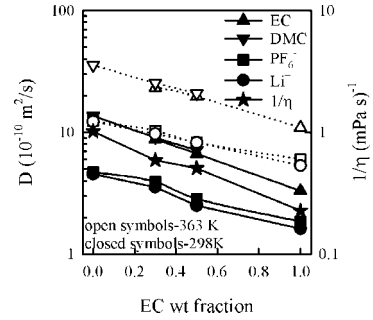

Figure 10. Ion and solvent self-diffusion coefficients and inverse viscosity for simulated electrolytes.

Ion and solvent self-diffusion coefficients as a function of solvent composition are shown in Figure 10. We find excellent agreement (<10% difference) between self-diffusion coefficients for small and large box simulations, indicating little finite size effect on ion dynamics. As expected, both ion and solvent diffusion monotonically increases with increasing fraction of DMC in a solvent. We note the similarity in the dependence of self-diffusion and inverse viscosity on solvent composition that can be seen in Figure 10.

Ionic conductivity from MD simulations is calculated using the Einstein relation

$$\lambda = \lim_{t\to\infty} \lambda^{\mathrm{app}}(t) = \lim_{t\to\infty} \frac{e^2}{6tVk_{\mathrm{B}}T} \sum_{i,j}^{N} z_i z_j \langle ([\mathbf{R}_i(t) - \mathbf{R}_i(0)])([\mathbf{R}_j(t) - \mathbf{R}_j(0)])\rangle \tag{13}$$

where e is the electron charge, V is the volume of the simulation box, k_{B} is Boltzmann's constant, T is the temperature, t is time, z_i and z_j are the charges over ions i and j in electrons, $\mathbf{R}_i(t)$ is the displacement of ion i during time t, the summation is performed over all ions, $\langle\rangle$ denotes the ensemble average, and N is the number of cations plus anions in the simulation cell. Here, $\lambda^{\mathrm{app}}(t)$ is the apparent time-dependent conductivity whose long-time limit corresponds to the equilibrium DC conductivity. Determining the long-time limit of $\lambda^{\mathrm{app}}(t)$ using eq 13 is problematic even at high temperatures where the diffusion coefficients can be accurately determined because $\lambda^{\mathrm{app}}(t)$, being a collective property, has poorer statistics and a higher uncertainty compared to MSD(t).

Conductivity can be decomposed into an "ideal" conductivity that would be realized if ion motion were uncorrelated, denoted $\lambda_{\mathrm{uncorr}}(t)$, and the degree to which ion motion is in fact uncorrelated, or α_{d}. The degree of uncorrelated ion motion is given as the ratio of the collective (total) charge transport (λ) to the charge transport due to self-diffusion only ($\lambda_{\mathrm{uncorr}}$)

$$\lambda_{\mathrm{uncorr}}^{\mathrm{app}} = \lim_{t\to\infty} \lambda_{\mathrm{uncorr}}^{\mathrm{app}}(t) = \lim_{t\to\infty} \frac{e^2}{6tVk_{\mathrm{B}}T} \sum_{i}^{n} z_i^2 \langle [\mathbf{R}_i(t) - \mathbf{R}_i(0)]^2 \rangle = \frac{e^2}{Vk_{\mathrm{B}}T}(n_+ D_+^{\mathrm{app}} + n_- D_-^{\mathrm{app}}) \tag{14}$$

$$\alpha_{\mathrm{d}} = \frac{\lambda}{\lambda_{\mathrm{uncorr}}} = \lim_{t\to\infty} \alpha_{\mathrm{d}}(t) = \lim_{t\to\infty} \frac{\lambda^{\mathrm{app}}(t)}{\lambda_{\mathrm{uncorr}}^{\mathrm{app}}(t)} \tag{15}$$

Here, n_i is the number of atoms of type i (Li^+ or $TFSI^-$) and $n = n_+ + n_-$. The degree of ion uncorrelated motion $\alpha_{\mathrm{d}} = 1$

corresponds to completely uncorrelated ion motion, while $\alpha_d = 0$ occurs if all of the cations only move together with anions. For practical reasons, we first determine α_d from the apparent $\alpha_d(t)$ plots shown in Figure 11. Our experience indicates that $\alpha_d(t)$ results are accurate only up to times approximately 1−2% of the total simulation run, consistent with similar claims for extracting viscosity from MD simulations.[70] Therefore, our best estimate of α_d in the long-time limit corresponds to the values taken from Figure 11 at times between 1 and 2% of the total simulated time given in Table 7.

Figure 11 indicates that α_d increases with decreasing temperature for EC/$LiPF_6$ and dramatically decreases with increasing DMC content. α_d vs electrolyte composition and temperature is shown in Figure 7 together with the (static) fraction of free ions from the structural analysis. We observe that α_d is always larger than the fraction of free ions from structural analysis, indicating an important contribution from charged ion clusters transport to ion conductivity as discussed above. Joint pgse-NMR and conductivity analysis of LiTFSI and $LiPF_6$ containing electrolytes found similar α_d values in γ-butyrolactone electrolyte.[73] A separate study of LiTFSI in multiple electrolytes at a solvent:Li ratio of 20 at 298 K for PC/LiTFSI and DMC/LiTFSI yielded α_d values 0.62 and 0.11.[8] Comparison of α_d extracted from our simulations with the experimental values gives indirect evidence that our simulation slightly overestimates α_d and hence the extent of $LiPF_6$ salt dissociation in EC/$LiPF_6$ electrolyte.

Ionic conductivity calculated from eq 15 using ion self-diffusion coefficients and α_d determined as discussed are shown in Figure 12. We observe that in EC/$LiPF_6$ and DMC/$LiPF_6$ our MD simulations overestimate conductivity by up to 37%, while conductivity of the mixed solvent electrolyte is in better agreement with experimental data. Figure 12a also shows that there is some disagreement between the two sets of experimental data shown. The slightly too high values obtained from our simulations for DC conductivity for EC/$LiPF_6$ may reflect an overestimation of salt dissociation as discussed above. However, we conclude that the observed agreement between MD simulation predictions and experimental data for DC conductivity in

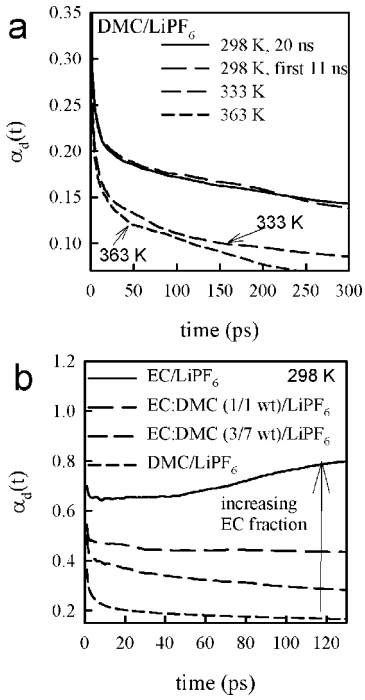

Figure 11. Apparent degree of ion uncorrelated motion (degree of dynamic ion dissociation).

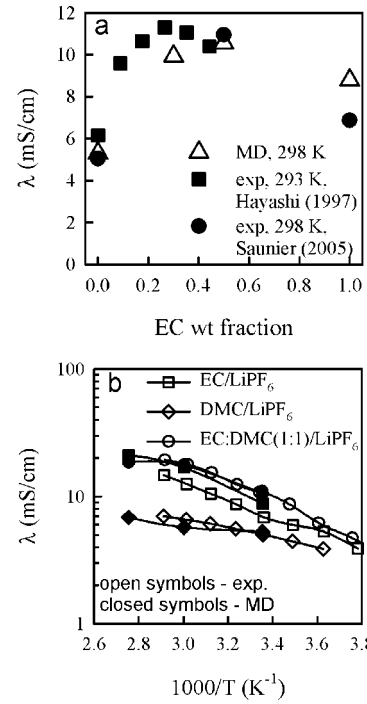

Figure 12. Concentration (a) and temperature (b) dependence of ion conductivity from MD simulations and experiments.[77,78]

EC, DMC, and mixed solvent electrolytes is quite good, particularly given the uncertainty in experimental data and difficulty in extracting α_d from simulations. Our estimations of DC conductivity represent a vast improvement over previous MD simulation predictions for carbonate electrolyte doped with $LiPF_6$[38] where simulations predicted a factor of 6 lower conductivity at 1 M $LiPF_6$ salt concentration. Finally, we point out that the maximum of ionic conductivity vs solvent composition is attributed to the faster increase of ion mobility (for free ions and charged aggregates) compared to the decrease of α_d with increasing DMC content of the electrolyte.

The solvent and anion residence times in the lithium first solvation shell have been analyzed in order to better understand Li^+ transport mechanisms in the pure and mixed electrolytes. The distribution of residence times for the solvent and anions to be present in the Li^+ first solvation shell were calculated using eq 16

$$P_{Li-X}(t) = \langle H(t)\, H(0)\rangle \qquad (16)$$

where $H(t)$ is 1 if a given species X = [Oc(DMC), Oc(EC), $P(PF_6^-)$] is involved in solvating a given Li^+ and zero otherwise. The brackets indicate averaging over all Li^+ and multiple time origins as well as normalization such that $P_{Li-X}(0) = 1$. The residence times for each species in the Li^+ solvation shell were calculated as the time integral of stretched exponential $\exp(-(t/\tau)^\beta)$ fits to the $P_{Li-X}(t)$ distribution functions and are shown in Figure 13. The Li−Oc(DMC) residence time is a factor of 1.6 longer than the Li−Oc(EC) residence time for DMC/$LiPF_6$ for the respective pure electrolytes. The slower exchange of DMC compared to EC around lithium also holds for the mixed solvents. This slower exchange could be due to the fact that Li^+ coordinated by DMC has a higher probability of having PF_6^- nearby whose slow exchange (see Figure 13) could hinder DMC solvent exchange. Additionally, isosurfaces of 3-D density distributions of carbonyl oxygen from EC and DMC

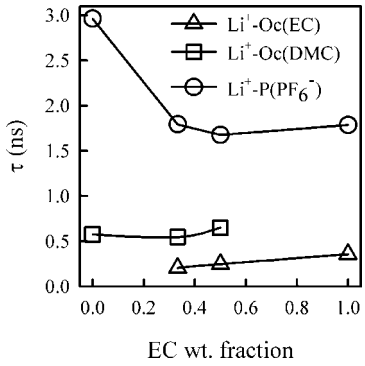

Figure 13. Residence times of carbonyl oxygen atoms for EC, DMC, and P of PF_6^- in the first lithium solvation shell. Atoms were considered to belong to the lithium first solvation shell if r(Li−Oc) < 2.8 Å and r(Li−P) < 4.4 Å.

around Li^+ (see Figure 3) clearly reveal a much wider probability surface for Oc(EC) compared to Oc(DMC) that could result in a smaller barrier for the EC exchange compared to the DMC exchange in the lithium first coordination shell.

The relatively long (1.5−3 ns) lifetime of Li^+−P coordination (see Figure 13) should be contrasted with the much faster decay of $P_{Li-F}(t)$, which has an associated lifetime on the order of 10 ps at 298 K. The approximately 2 orders of magnitude difference between the Li^+−P residence time and Li^+−F residence time demonstrates that Li^+−F coordination exchanges with fluorine atoms on the same PF_6^- anion occur hundreds of times before the PF_6^- anion finally leaves the first lithium coordination shell. Such behavior is consistent with very fast rotation of PF_6^- anions as obtained from the P−F bond vector autocorrelation function, which exhibits an autocorrelation time on the order of 10 ps for all electrolytes investigated.

In the final part of our analysis, we calculate an average displacement that a lithium cation undergoes during one Li^+-solvent residence (τ_{res}) time at 298 K. We obtain 5.8 and 12.3 Å lithium displacements during τ_{res} for EC/$LiPF_6$ and DMC/$LiPF_6$, respectively. The approximate sizes of EC and DMC are 4.2 and 6.2 Å, measured as the largest distance between any two atoms in a molecule. Following analysis from our previous work[36] and comparing the molecule size to the Li^+-solvent residence time, we conclude that Li^+ motion in EC/$LiPF_6$ occurs by a comparable contribution from Li^+ moving together with its solvation shell and by exchange of solvent molecules. The much larger distance traveled by a Li^+ in DMC/$LiPF_6$ before solvent exchange indicates that in this electrolyte Li^+ motion occurs primarily by moving together with its solvation shell, similar to our findings[36] for 1,2-dimethoxyethane, another low dielectric constant solvent.

VII. Conclusions

Quantum chemistry calculations on gas-phase solvent (EC and DMC)−ion complexes and MD simulation of liquid electrolytes provide a consistent picture of the lithium solvation in mixed EC:DMC/$LiPF_6$ electrolytes. Quantum chemistry calculations performed on solvent−ion clusters reveal that the energy for EC substitution with DMC decreases with increasing number of solvent molecules coordinating Li^+. For the largest gas-phase complex investigated, we find that the EC_4/Li^+ complex is not the most energetically stable, but instead, the EC_3DMC/Li^+ complex was found to be the most energetically stable. The high energy cis−trans conformer of DMC forms a more energetically stable complex with Li^+ than the gas-phase low energy cis−cis DMC conformer. Addition of the anion to the solvent−cation complex revealed that the DMC/$LiPF_6$ complex is slightly lower in energy than EC/$LiPF_6$, indicating that the presence of the PF_6^- anion in the liquid electrolyte might strongly influence the relative stability of EC vs DMC cation coordination.

A transferable quantum chemistry-based polarizable force field has been developed based in part upon these quantum chemistry studies. Its ability to reproduce relative binding energies of solvent−ion complexes has been validated. Moreover, thermodynamic and transport properties of EC and DMC solvent were predicted in excellent agreement with experiment. The predicted conductivity of DMC/$LiPF_6$, EC/$LiPF_6$, and mixed solvent electrolytes doped with $LiPF_6$ was also found to be in good agreement with experiment. Structural analysis of mixed EC:DMC 1 M $LiPF_6$ electrolytes indicated a slightly higher probability for finding DMC vs EC molecules in the lithium first solvation shell compared to the expected results from random mixing. A more detailed examination of the mixed electrolytes also revealed that the free cations favor equal DMC and EC solvation, while Li^+ in contact with PF_6^- anions leads to a preference for DMC in the Li^+ solvation shell.

A monotonic increase in the fraction of free (uncomplexed by a counterion) ions and a monotonic decrease in ion and solvent diffusion coefficients with increasing EC content of the solvent was observed, leading to a maximum in conductivity for the mixed electrolyte. For all electrolytes, a significant contribution to conductivity from charged ion aggregates was found, with this contribution increasing with increasing DMC fraction in the electrolyte.

Acknowledgment. We thank Richard Jow (ARL) and John Kerr (LBNL) for helping us to define electrolytes for investigation and properties to explore. Qin Liu's help with running some quantum chemistry jobs is acknowledged. Dmitry Bedrov's suggestion to perform MD simulations of mixed electrolytes with an artificially increased Li^+/PF_6^- repulsion is highly appreciated. The author is grateful for financial support of this work by the Assistant Secretary for Energy Efficiency and Renewable Energy, Office of FreedomCAR and Vehicle Technologies of the U.S. Department of Energy under Contract No. DE-AC02-05CH11231 on PO No. 6838611 (University of Utah) and US Army support to WMI through W911QX-07-P-0602.

Supporting Information Available: Figures of EC_nDMC_m/Li^+ ($n + m = 3, 4$) complexes optimized at the M05-2X/6-31G* level. This material is available free of charge via the Internet at http://pubs.acs.org.

References and Notes

(1) Armand, M.; Tarascon, J. M. *Nature* **2008**, *451*, 652.
(2) Xu, K. *Chem. Rev.* **2004**, *104*, 4303.
(3) Arai, J.; Nishimura, K.; Muranaka, Y.; Ito, Y. *J. Power Sources* **1997**, *68*, 304.
(4) Valoen, L. O.; Reimers, J. N. *J. Electrochem. Soc.* **2005**, *152*, A882.
(5) Brouillette, D.; Perron, G.; Desnoyers, J. E. *J. Solution Chem.* **1998**, *27*, 151.
(6) Matsubara, K.; Kaneuchi, R.; Maekita, N. *J. Chem. Soc., Faraday Trans.* **1998**, *94*, 3601.
(7) Blomgren, G. E. *J. Power Sources* **1999**, *82*, 112.
(8) Hayamizu, K.; Aihara, Y.; Arai, S.; Martinez, C. G. *J. Phys. Chem. B* **1999**, *103*, 519.
(9) Katayama, H.; Arai, J.; Akahoshi, H. *J. Power Sources* **1999**, *82*, 705.
(10) Zhang, S. S.; Xu, K.; Jow, T. R. *J. Power Sources* **2006**, *154*, 276.
(11) Zhang, S. S.; Xu, K.; Jow, T. R. *J. Power Sources* **2006**, *159*, 702.
(12) Ding, M. S.; Jow, T. R. *J. Electrochem. Soc.* **2005**, *152*, A1199.
(13) Ding, M. S.; Xu, K.; Zhang, S. S.; Amine, K.; Henriksen, G. L.; Jow, T. R. *J. Electrochem. Soc.* **2001**, *148*, A1196.

(14) Zhang, S. S.; Jow, T. R.; Amine, K.; Henriksen, G. L. *J. Power Sources* **2002**, *107*, 18.
(15) Xu, K.; Lam, Y. F.; Zhang, S. S.; Jow, T. R.; Curtis, T. B. *J. Phys. Chem. C* **2007**, *111*, 7411.
(16) Ding, M. S.; Jow, T. R. *J. Electrochem. Soc.* **2004**, *151*, A2007.
(17) Ding, M. S.; Jow, T. R. *J. Electrochem. Soc.* **2003**, *150*, A620.
(18) Zhang, S. S.; Xu, K.; Jow, T. R. *J. Solid State Electrochem.* **2003**, *7*, 147.
(19) Reddy, V. P.; Smart, M. C.; Chin, K. B.; Ratnakumar, B. V.; Surampudi, S.; Hu, J. B.; Yan, P.; Prakash, G. K. S. *Electrochem. Solid-State Lett.* **2005**, *8*, A294.
(20) Ding, M. S.; Xu, K.; Jow, T. R. *J. Electrochem. Soc.* **2000**, *147*, 1688.
(21) Ding, M. S.; Xu, K.; Zhang, S. S.; Jow, T. R. *J. Electrochem. Soc.* **2001**, *148*, A299.
(22) Kameda, Y.; Umebayashi, Y.; Takeuchi, M.; Wahab, M. A.; Fukuda, S.; Ishiguro, S. I.; Sasaki, M.; Amo, Y.; Usuki, T. *J. Phys. Chem. B* **2007**, *111*, 6104.
(23) Wang, Y. X.; Balbuena, P. B. *Int. J. Quantum Chem.* **2005**, *102*, 724.
(24) Li, T.; Balbuena, P. B. *J. Electrochem. Soc.* **1999**, *146*, 3613.
(25) Wang, Y. X.; Nakamura, S.; Ue, M.; Balbuena, P. B. *J. Am. Chem. Soc.* **2001**, *123*, 11708.
(26) Wang, Y. X.; Balbuena, P. B. *J. Phys. Chem. A* **2001**, *105*, 9972.
(27) Johansson, P. *Phys. Chem. Chem. Phys.* **2007**, *9*, 1493.
(28) Vollmer, J. M.; Curtiss, L. A.; Vissers, D. R.; Amine, K. *J. Electrochem. Soc.* **2004**, *151*, A178.
(29) Masia, M.; Rey, R. *J. Phys. Chem. B* **2004**, *108*, 17992.
(30) Masia, M.; Probst, M.; Rey, R. *J. Phys. Chem. B* **2004**, *108*, 2016.
(31) Soetens, J. C.; Millot, C.; Maigret, B. *J. Phys. Chem. A* **1998**, *102*, 1055.
(32) Silva, L. B.; Freitas, L. C. G. *THEOCHEM* **2007**, *806*, 23.
(33) Borodin, O.; Smith, G. D. *J. Phys. Chem. B* **2006**, *110*, 4971.
(34) Borodin, O.; Smith, G. D. *J. Phys. Chem. B* **2006**, *110*, 6279.
(35) Borodin, O.; Smith, G. D. *J. Phys. Chem. B* **2006**, *110*, 6293.
(36) Borodin, O.; Smith, G. D. *J. Solution Chem.* **2007**, *36*, 803.
(37) Tasaki, K.; Nakamura, S. *J. Electrochem. Soc.* **2001**, *148*, A984.
(38) Newman, J.; Thomas, K. E.; Hafezi, H.; Wheeler, D. R. *J. Power Sources* **2003**, *119*, 838.
(39) Matsuda, Y.; Fukushima, T.; Hashimoto, H.; Arakawa, R. *J. Electrochem. Soc.* **2002**, *149*, A1045.
(40) Morita, M.; Asai, Y.; Yoshimoto, N.; Ishikawa, M. *J. Chem. Soc., Faraday Trans.* **1998**, *94*, 3451.
(41) Borodin, O.; Smith, G. D.; Geiculescu, O.; Creager, S. E.; Hallac, B.; DesMarteau, D. *J. Phys. Chem. B* **2006**, *110*, 24266.
(42) Siqueira, L. J. A.; Ribeiro, M. C. C. *J. Chem. Phys.* **2006**, *125*, 214903.
(43) Li, S.; Cao, Z.; Peng, Y. X.; Liu, L.; Wang, Y. L.; Wang, S.; Wang, J. Q.; Yan, T. Y.; Gao, X. P.; Song, D. Y.; Shen, P. W. *J. Phys. Chem. B* **2008**, *112*, 6398.
(44) Brandell, D.; Liivat, A.; Aabloo, A.; Thomas, J. O. *J. Mater. Chem.* **2005**, *15*, 4338.
(45) Brandell, D.; Liivat, A.; Kasemagi, H.; Aabloo, A.; Thomas, J. O. *J. Mater. Chem.* **2005**, *15*, 1422.
(46) Borodin, O.; Smith, G. D.; Jaffe, R. L. *J. Comput. Chem.* **2001**, *22*, 641.
(47) Frisch, M. J.; et al. Gaussian 03, revision E1; Gaussian, Inc.: Pittsburgh, PA, 1998.
(48) Zhao, Y.; Truhlar, D. G. *J. Chem. Phys.* **2006**, *125*, 194101.
(49) Zheng, J. J.; Zhao, Y.; Truhlar, D. G. *J. Phys. Chem. A* **2007**, *111*, 4632.
(50) Shao, Y.; Molnar, L. F.; Jung, Y.; Kussmann, J.; Ochsenfeld, C.; Brown, S. T.; Gilbert, A. T. B.; Slipchenko, L. V.; Levchenko, S. V.; O'Neill, D. P.; DiStasio, R. A.; Lochan, R. C.; Wang, T.; Beran, G. J. O.; Besley, N. A.; Herbert, J. M.; Lin, C. Y.; Van Voorhis, T.; Chien, S. H.; Sodt, A.; Steele, R. P.; Rassolov, V. A.; Maslen, P. E.; Korambath, P. P.; Adamson, R. D.; Austin, B.; Baker, J.; Byrd, E. F. C.; Dachsel, H.; Doerksen, R. J.; Dreuw, A.; Dunietz, B. D.; Dutoi, A. D.; Furlani, T. R.; Gwaltney, S. R.; Heyden, A.; Hirata, S.; Hsu, C. P.; Kedziora, G.; Khalliulin, R. Z.; Klunzinger, P.; Lee, A. M.; Lee, M. S.; Liang, W.; Lotan, I.; Nair, N.; Peters, B.; Proynov, E. I.; Pieniazek, P. A.; Rhee, Y. M.; Ritchie, J.; Rosta, E.; Sherrill, C. D.; Simmonett, A. C.; Subotnik, J. E.; Woodcock, H. L.; Zhang, W.; Bell, A. T.; Chakraborty, A. K.; Chipman, D. M.; Keil, F. J.; Warshel, A.; Hehre, W. J.; Schaefer, H. F.; Kong, J.; Krylov, A. I.; Gill, P. M. W.; Head-Gordon, M. *Phys. Chem. Chem. Phys.* **2006**, *8*, 3172.
(51) Zhao, Y.; Truhlar, D. G. *Org. Lett.* **2006**, *8*, 5753.
(52) Zhao, Y.; Truhlar, D. G. *J. Org. Chem.* **2007**, *72*, 295.
(53) Zhao, Y.; Truhlar, D. G. *J. Chem. Theory Comput.* **2006**, *2*, 1009.
(54) Zhao, Y.; Truhlar, D. G. *J. Chem. Theory Comput.* **2007**, *3*, 289.
(55) Zhao, Y.; Schultz, N. E.; Truhlar, D. G. *J. Chem. Theory Comput.* **2006**, *2*, 364.
(56) Zhao, Y.; Truhlar, D. G. *J. Phys. Chem. A* **2008**, *112*, 1095.
(57) Smith, G. D.; Jaffe, R. L.; Partridge, H. *J. Phys. Chem. A* **1997**, *101*, 1705.
(58) Borodin, O. APPLE&P (Atomistic Polarizable Potential for Liquids, Electrolytes and Polymers), rev 1e; www.wasatchmolecular.com.
(59) Pierce, F.; Tsige, M.; Borodin, O.; Perahia, D.; Grest, G. S. *J. Chem. Phys.* **2008**, *128*, 214903.
(60) Borodin, O.; Smith, G. D. *J. Phys. Chem. B* **2006**, *110*, 11481.
(61) Borodin, O.; Smith, G. D.; Fan, P. *J. Phys. Chem. B* **2006**, *110*, 22773.
(62) Borodin, O.; Smith, G. D.; Henderson, W. *J. Phys. Chem. B* **2006**, *110*, 16879.
(63) Smith, G. D.; Borodin, O.; Li, L.; Kim, H.; Liu, Q.; Bara, J. E.; Gin, D. L.; Nobel, R. *Phys. Chem. Chem. Phys.* **2008**, *10*, 6301.
(64) Morita, A.; Kato, S. *J. Chem. Phys.* **1999**, *110*, 11987.
(65) Ayyagari, C.; Bedrov, D.; Borodin, O.; Smith, G. D. Lucretius, MD simulation code; http://www.eng.utah.edu/~gdsmith/lucretius.html.
(66) Frenkel, D.; Smit, B. *Understanding Molecular Simulation: From Algorithms to Applications*, 2nd ed.; Academic Press: San Diego, 2002.
(67) Burba, C. M.; Frech, R. *J. Phys. Chem. B* **2005**, *109*, 15161.
(68) Dunweg, B.; Kremer, K. *J. Chem. Phys.* **1993**, *99*, 6983.
(69) Daivis, P. J.; Evans, D. J. *J. Chem. Phys.* **1994**, *100*, 541.
(70) Mondello, M.; Grest, G. S. *J. Chem. Phys.* **1997**, *106*, 9327.
(71) Bedrov, D.; Smith, G. D.; Sewell, T. D. *J. Chem. Phys.* **2000**, *112*, 7203.
(72) Hayamizu, K.; Aihara, Y. *Electrochim. Acta* **2004**, *49*, 3397.
(73) Aihara, Y.; Bando, T.; Nakagawa, H.; Yoshida, H.; Hayamizu, K.; Akiba, E.; Price, W. S. *J. Electrochem. Soc.* **2004**, *151*, A119.
(74) http://www.hbcpnetbase.com/; The CRC Handbook of Chemistry and Physics, 2006−2007.
(75) Steele, W. V.; Chirico, R. D.; Knipmeyer, S. E.; Nguyen, A. *J. Chem. Eng. Data* **1997**, *42*, 1008.
(76) Lamoureux, G.; MacKerell, A. D.; Roux, B. *J. Chem. Phys.* **2003**, *119*, 5185.
(77) Hayashi, K.; Nemoto, Y.; Tobishima, S.; Yamaki, J. *J. Power Sources* **1997**, *68*, 316.
(78) Saunier, J.; Gorecki, W.; Alloin, F.; Sanchez, J. Y. *J. Phys. Chem. B* **2005**, *109*, 2487.

JP809614H